IN SITU MEASUREMENT OF GAS-SOLID INTERACTIONS IN ASTROPHYSICAL DUST & PLANETARY ANALOGUES

S.P. Thompson[1], J.E. Parker[1], S.J. Day[1,2], A. Evans[2] and C.C. Tang[1]

Abstract. Facilities for studying gas-solid interactions on beamline I11 at the Diamond Light Source are described. Sample evolution in low and high gas pressure capillary cells (1×10^{-7} to 100 bar) with non-contact cooling and heating (80 to 1273 K) can be monitored structurally (X-rays) and spectroscopically (Raman). First results on the dehydration of $MgSO_4.7H_2O$, the formation of CO_2 clathrate hydrate and the reaction of amorphous $CaSiO_3$ grains with CO_2 gas to form $CaCO_3$ are presented to demonstrate the application of these cells to laboratory investigations involving the processing of cosmic dust simulants and planetary materials analogues.

1 Introduction

Beamline I11 at Diamond is designed for high resolution and time-resolved *in situ* synchrotron X-ray scattering measurements (Thompson *et al.* 2009, 2011). We have recently constructed two reaction cells for studying gas-solid interactions in powder samples at low ($\lesssim1.5$ bar) and high (<100 bar) gas pressures, with a 532 nm Raman system (Horiba) providing additional in situ spectroscopic data. Here we describe the design and operational characteristics of the cells and present a number of representative first results aimed at demonstrating their application to the laboratory study of the in situ processing of analogue materials of astrophysical and planetary interest. Specifically we follow (i) the dehydration of magnesium sulphate which represents a likely constituent of planetary surfaces; (ii) the formation of CO_2 clathrate hydrate which is a proposed constituent and gas sequestrator in comets and planetary surfaces and (iii) the dry non-aqueous formation of calcium carbonate, known to be a solid phase component of certain circumstellar regions, by the carbonation of amorphous Ca-silicate bearing grains by CO_2 gas.

---

[1] Diamond Light Source, Chilton, Didcot, Oxon OX11 0DE, UK

[2] Astrophysics Group, Keele University, Staffs ST5 5BG, UK
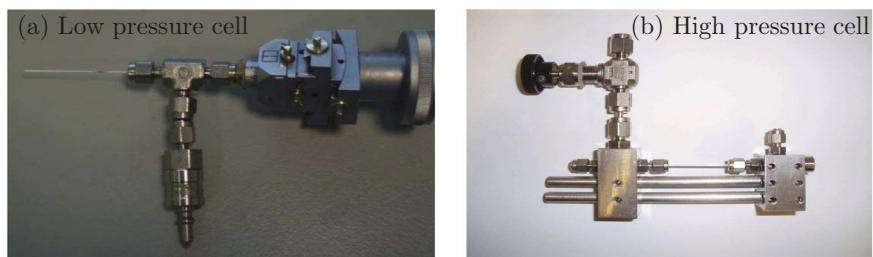
Fig. 1. Capillary gas reaction cells developed for beamline I11 at Diamond Light Source.

2   Gas cell design and experimental arrangement

The low pressure cell (LPC, Fig. 1a) comprises a $\frac{1}{16}$" T-piece capped at one end by a stub for goniometer mounting and alignment. The inlet side connects to a gas control system (Parker *et al.* 2012) via a self sealing quick-connect fitting. The outlet side holds a borosilicate, or for T > 815° C a quartz, capillary sealed into a Swagelok fitting via a vespel ferrule drilled to match the capillary diameter (0.5–0.7 mm). The high pressure cell (HPC, Fig. 1b) similarly employs $\frac{1}{16}$" Swagelok fittings, but these are mounted in a type 316 stainless steel body with bracing supports. Sealing is again by vespel ferrule, with samples loaded inside a 1 mm diameter quartz or single crystal sapphire tube. The HPC can also be used in flow mode by removing a blank in the cell body. The gas control system includes a turbo pump allowing evolved gases to be removed, or for multiple gas dosing/evacuation cycles to be run. In both cells a quartz wool plug inserted into the end of the capillary or tube prevents sample loss during evacuation.

The cells mount on the central θ-circle of a vertical concentric three-circle diffractometer and are aligned with the instrument's centre of rotation, which is coincident with the incoming X-ray beam. Five angle-scanning high resolution multi-analyzer crystal (MAC) stages sit on the 2θ-circle and a 90° arc position sensitive detector (PSD) is located on the outer δ-circle. The θ-circle can also oscillate the cell capillary ±10° about its axis to improve sampling statistics. The Raman probe (65 mm working distance) is mounted on a separate linear drive located on a sample table next to the diffractometer and connects to a iHR550 imaging spectrometer. Once an X-ray measurement is completed, the MACs/PSD move to parked positions and the Raman probe drives in. Thus ongoing structural and spectroscopic data collection can be interleaved as gas injection and/or temperature are varied. Alternatively, sample evolution can be monitored by X-rays or Raman until a point of interest is reached and the systems swapped. Typical Raman collection times can be seconds to minutes, while X-ray collection by the PSD can be sub-second to tens of seconds and for the MACs 2–60 minutes. Non-contact cooling and heating covering 80–1273 K is provided by a liquid nitrogen Cryostream Plus (Oxford Cryosystems) or a hot air blower (Cyberstar), with maximum ramp rates of 6 and 10 K per minute respectively.

3 First results

3.1 Dehydration of MgSO$_4$.7H$_2$O magnesium sulphate

The rocky cores and mantles of Jupiter's large icy moons likely formed from chondritic materials, from which MgSO$_4$ occurs as a leachate (Kargel 1991). It also possibly occurs as brine, from subsurface reservoirs, on Europa and Ganymede (Orlando *et al.* 2005) and may be present in carbonatite lavas on Venus (Kargel *et al.* 1994). Similar hydrated salts likely exist on large outer asteroids (McCord & Sotin 2005) and in the sulphate-rich sedimentary rocks that are widespread on Mars (Moore *et al.* 2010). MgSO$_4$.nH$_2$O can adopt various $n = 0.12$ hydration states, but the pathways between them and their relative stabilities are complex and depend strongly on environmental conditions (Wang *et al.* 2009). A sample of reagent grade MgSO$_4$.7H$_2$O (epsomite) powder was heated in the LPC over a range of temperatures and Raman spectra (10 s each, Fig. 2a) and X-ray PSD patterns (4 s each, $\lambda = 0.826098$ Å, Fig. 2b) were collected. The Raman feature at 980–1030 cm^{-1} is characteristic of hydration state, with the shifts in position suggesting a dehydration path up to 110°C of 7H$_2$O $\rightarrow$ 6H$_2$O $\rightarrow$ 4/5H$_2$O $\rightarrow$ 4H$_2$O. Above 50°C mixed phase PSD patterns confirm hexahydrite ($n = 6$), pentahydrite ($n = 5$) and starkeyite ($n = 4$) form as structural change accompanies dehydration.

3.2 Formation of CO$_2$ clathrate hydrate

Clathrate hydrates incorporate gas molecules within cages of H$_2$O ice and may explain primordial noble gas depletion on Titan (Mousis *et al.* 2011), while their dissociation during cryovolcanism could be the source of Titan's atmospheric methane replenishment (Tobie *et al.* 2006) as well as polar CH$_4$, N$_2$, CO$_2$ and H$_2$O plumes on Enceladus (Kieffer *et al.* 2006) and seasonal methane plumes on Mars (Mumma *et al.* 2003). SO$_2$, CO$_2$, CH$_4$ and H$_2$S clathrates should be stable on the surface/oceans of Europa (Prieto-Ballesteros *et al.* 2005) and CO, CO$_2$, CH$_4$ and H$_2$S clathrates may form in certain comets (Marboeuf *et al.* 2011). Demineralised water was frozen at 200 K in the HPC and Fig. 2c (bottom) shows PSD data below the first ice peak (2 s, $\lambda = 0.826163$ Å), before progressively injecting CO$_2$ at 1.8, 7.6 and 38 bar, forming weak clathrate features (Fig. 2c). Figure 2d shows a final 10 s exposure at 42 bar. Peak positions did not vary with pressure and from the first 6 peaks a lattice parameter of 14.0 ± 0.5 Å was obtained, which is longer than usually reported (11.8 Å) possibly due to formation being a two step process: a fast initial conversion rate followed by a slower diffusion-limited rate (Henning *et al.* 2000). The low initial pressure does not give complete conversion from hexagonal ice to cubic sI hydrate, with slow CO$_2$ diffusion through this structure inhibiting further conversion, even at increased pressures. CO$_2$ was then injected at 20 bar into fresh ice at 220 K to form clathrate and the temperature slowly raised (ΔT = 1 K above 245 K). The ice peaks weakened and the clathrate peaks increased in strength, until 252 K when the ice disappeared leaving only the clathrate (Fig. 2e) with a lattice parameter for this initial injection pressure close to the 11.8 Å of sI hydrate.
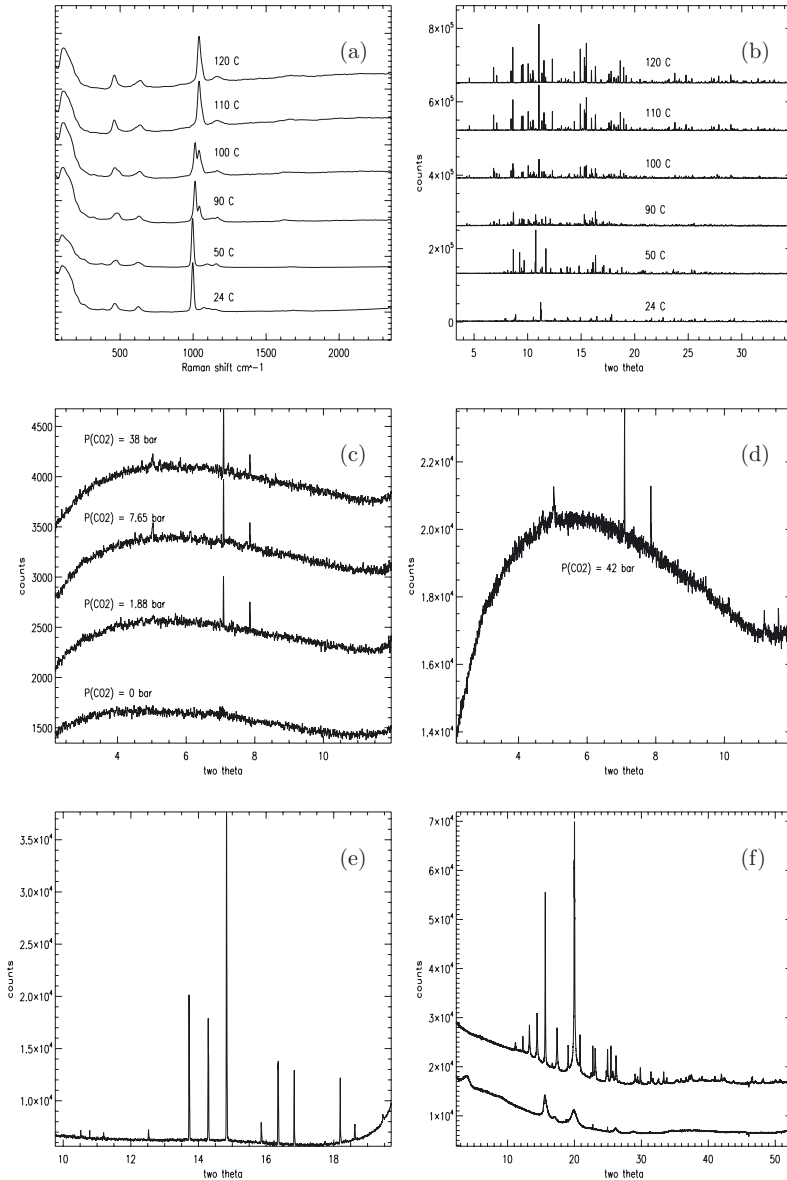
Fig. 2. *In situ* Raman and X-ray diffraction data collected using the pressure cells: (a) Raman spectra and (b) X-ray diffraction data showing the dehydration of $MgSO_4.7H_2O$ with increasing temperature; (c) and (d) X-ray diffraction patterns showing formation of CO_2 clathrate hydrate in water ice via the injection of CO_2 gas; (e) diffraction pattern of the clathrate phase following the removal of ice by melting; (f) X-ray diffraction patterns showing the formation of crystalline calcium carbonate ($CaCO_3$, top pattern) following the reaction of CO_2 gas with amorphous $CaSiO_3$ silicate grains (bottom pattern).

3.3   Calcium carbonate CaCO$_3$ formation by CaSiO$_3$-CO$_2$ gas interaction

Terrestrial carbonates form by silicate weathering in watery CO_2^{3-} solutions. However observations show the presence of carbonate features in debris-disks, certain circumstellar regions and planetary nebulae (*e.g.* Chiavassa *et al.* 2005), none of which contain liquid water. Furthermore, direct carbonate condensation is suppressed by silicate grain outflow (Ferrarotti & Gail 2005). Stellar carbonates could however potentially form via reactions between Ca-bearing silicate grains and CO_2 gas. Using the HPC, fine-grained amorphous CaSiO$_3$ powder (Thompson *et al.* 2012) at ambient temperature was injected with CO_2 at 6 bar. Figure 2f (bottom) shows the amorphous CaSiO$_3$ diffraction pattern (10 s, $\lambda = 0.826422$ Å) before injection (the peak at 20° 2θ is from the sapphire tube) and Figure 2f (top) shows the post-injection formation of a crystalline CaCO$_3$ phase. Further experiments showed the required gas pressure and conversion rate at fixed temperature depend on sample packing within the cell. Work is currently ongoing into the kinetics and structural mechanism of formation in both this Ca-silicate and mixed composition $Mg_xCa_{1-x}SiO_3$ silicates (see also Day *et al.*, these proceedings).

References

Chiavassa, A., Ceccarelli, C., Tielens, A.G.G.M, Caux, E., & Maret, S., 2005, A&A, 432, 547

Ferrarotti, A.S., & Gail, H.-P., 2005, A&A, 430, 959

Henning, R.W., Schultz, A.J., Thieu, Vu., & Halpern, Y., 2000, J. Phys. Chem. A, 104, 5066

Kargel, J.S., 1991, Icarus, 94, 368

Kargel, J.S., Kirk, R.L., Fegley, B., & Treiman, A.H., 1994, Icarus, 112, 219

Kieffer, S.W., Lu, X., Bethke, C.M., *et al.*, 2006, Science, 314, 1764

Marboeuf, U., Mousis, O., Petit, J.-M., *et al.*, 2011, A&A, 525, A144

McCord, T.B., & Sotin, C., 2005, J. Geophys. Res., 110, E05009

Moore, J.M., Bullock, M.A., Newsom, H., & Nelson, M., 2010, J. Geophys. Res., 115, E06009

Mousis, O., Lunine, J.I., Picaud, S., *et al.*, 2011, ApJ, 740, L9

Mumma, M.J., Villanueva, G.L., Novak, R.E., *et al.*, 2003, Science, 323, 1041

Orlando, T.M., McCord, T.B., & Grieves, G.A., 2005, Icarus, 177, 528

Parker, J.E., Potter, J., Thompson, S.P., Lennie, A.R., & Tang, C.C., 2012, Mater. Sci. Forum, 706, 1707

Prieto-Ballesteros, O., Kargel, J.S., Fernández-Sampedro, M., *et al.*, 2005, Icarus, 177, 491

Thompson, S.P., Parker, J.E., Potter, J., *et al.*, 2009, Rev. Sci. Instr., 80

Thompson, S.P., Parker, J.E., Marchal, J., *et al.*, 2011, J. Synchrotron Rad., 18, 637

Thompson, S.P., Day, S.J., Parker, J.E., Evans, A.E., & Tang, C.C., 2012, J. Non-Cryst. Solids, 358, 885

Tobie, G., Lunine, J.I., & Sotin, C., 2006, Nature, 440, 61

Wang, A., Freeman, J.J., & Jolliff, B.L., 2009, J. Geophys. Res., 114, E04010